

A possible origin of viscosity in Keplerian accretion disks due to secondary perturbation: Turbulent transport without magnetic fields

Banibrata Mukhopadhyay and Kanak Saha

Astronomy and Astrophysics Program, Department of Physics, Indian Institute of Science, Bangalore 560012, India; bm@physics.iisc.ernet.in

Received 2010 August 13; accepted 2010 September 1

Abstract The origin of hydrodynamic turbulence in rotating shear flow is a long standing puzzle. Resolving it is especially important in astrophysics when the flow's angular momentum profile is Keplerian which forms an accretion disk having negligible molecular viscosity. Hence, any viscosity in such systems must be due to turbulence, arguably governed by magnetorotational instability, especially when temperature $T \gtrsim 10^5$. However, such disks around quiescent cataclysmic variables, protoplanetary and star-forming disks, and the outer regions of disks in active galactic nuclei are practically neutral in charge because of their low temperature, and thus are not expected to be coupled with magnetic fields enough to generate any transport due to the magnetorotational instability. This flow is similar to plane Couette flow including the Coriolis force, at least locally. What drives their turbulence and then transport, when such flows do not exhibit any unstable mode under linear hydrodynamic perturbation? We demonstrate that the three-dimensional secondary disturbance to the primarily perturbed flow that triggers elliptical instability may generate significant turbulent viscosity in the range $0.0001 \lesssim \nu_t \lesssim 0.1$, which can explain transport in accretion flows.

Key words: accretion, accretion disks — hydrodynamics — turbulence — instabilities

1 INTRODUCTION

One of the main problems behind the origin of hydrodynamic turbulence in shear flow is that there is a significant mismatch between the predictions of linear theory and experimental data. For example, in the case of plane Couette flow, laboratory experiments and numerical simulations show that the flow may be turbulent at a Reynolds number as low as $Re \sim 350$, but according to linear theory, the flow should be stable for all Re . Similar mismatch between theoretical results and observations is found in astrophysical contexts, where the accretion flow of neutral gas with a Keplerian angular momentum profile, which essentially behaves like rotating shear flow, is a common subject. Examples of such flow systems are accretion disks around quiescent cataclysmic variables (Gammie & Menou 1998), protoplanetary and star-forming disks (Blaes & Balbus 1994), and the outer regions of disks in active galactic nuclei (Menou & Quataert 2001).

A Keplerian accretion disk flow having a very low molecular viscosity must generate turbulence and successively diffusive viscosity, which supports the transfer of mass inwards and angular momentum outwards. However, theoretically this flow, in the absence of magnetic fields, never exhibits any unstable mode which could trigger turbulence in the system. On the other hand, laboratory experiments of Taylor-Couette systems, which are similar to Keplerian disks, seem to indicate that although the Coriolis force delays the onset of turbulence, the flow is ultimately unstable with respect to turbulence for Reynolds numbers larger than a few thousand (Richard & Zahn 1999), even for subcritical systems. Indeed, Bech & Andersson (1997) see turbulence persisting in numerical simulations of subcritical rotating flows for large enough Reynolds numbers.

How does shearing flow that is linearly stable to perturbations switch to a turbulent state? Since the last decade, many authors, including ourselves, have come forward with a possible explanation of this fact based on a *bypass* transition (see Butler & Farrell 1992; Reddy & Henningson 1993; Trefethen et al. 1993; Chagelishvili et al. 2003; Umurhan & Regev 2004; Mukhopadhyay et al. 2005 and references therein) where the decaying linear modes show an arbitrarily large transient energy growth at a suitably tuned perturbation. In lieu of linear instabilities, e.g. magnetorotational instability, and the transient energy growth, supplemented by a non-linear feedback process to repopulate the growing disturbance, could plausibly sustain turbulence for large enough Reynolds numbers.

The behavior of shear flows, however, in the presence of rotation is enormously different compared to that in the absence of rotation. The Coriolis effect is the main culprit behind this change in behavior, killing any growth of energy, even of the transient kind, in the presence of rotation. In the case of shear flow with a varying angular velocity profile, like Keplerian accretion flow, the above mentioned transient energy growth is insignificant for three-dimensional perturbations. To overcome this limitation, it is necessary to invoke additional effects. Various kinds of secondary instability, such as the elliptical instability, are widely discussed as a possible route to self-sustained turbulence in linearly perturbed shear flows (see, e.g. Pierrehumbert 1986; Bayly 1986; Craik & Criminale 1986; Landman & Saffman 1987; Hellberg & Orszag 1988; Waleffe 1990; Craik 1989; Le Dizès et al. 1996; Kerswell 2002). These effects, which generate three-dimensional instabilities of a two-dimensional flow with elliptical streamlines, have been proposed as a generic mechanism for the breakdown of many two-dimensional high Reynolds number flows whose vortex structures can be locally characterized as elliptical streamlines. Recently, one of the present authors has studied the secondary perturbation and corresponding elliptical vortex effects in accretion disks and pointed out that they can be the seed of three-dimensional hydrodynamic instability (Mukhopadhyay 2006). Subsequently, by numerical simulation, this has been shown to be one of the possible sources that can generate turbulence to form large objects from the dusty gas surrounding a young star (Cuzzi 2007; Ormel et al. 2008). Moreover, hydrodynamic turbulence can generate vortex activity in unmagnetized protoplanetary disks (de Val-Borro et al. 2007), which leads to planet formation and angular momentum transport in disks. However, whether they lead to non-linear feedback and three-dimensional turbulence have yet to be explicitly demonstrated.

Here we plan to show in detail that three-dimensional secondary perturbation causing large growth in the flow time scale may generate significant turbulent viscosity in rotating shear flows; more precisely, in plane shear flows in the presence of the Coriolis force. The plane shear flow with the Coriolis force essentially behaves like a local patch of a rotating shear flow. The possibility of significant turbulent transport in such flows by three-dimensional perturbation opens a new window to explain the accretion process in flows which are neutral in charge. In particular, we address the issue of deriving turbulent viscosity and the Shakura-Sunyaev viscosity parameter α (Shakura & Sunyaev 1973) from a pure hydrodynamical perspective¹. This is important for understanding accretion flows in a cold charge-neutral medium.

¹ A preliminary calculation of such α has appeared in a collected volume of the Gravity Research Foundation (Mukhopadhyay 2008).

It is important to note that the transition to turbulence is not a unique process, but it depends on the initial condition/disturbance and the nature of the flow (Schmid & Henningson 2001; Criminale et al. 2003). In fact, it is known that even in the presence of secondary instability, linearly unstable base flows may reach a non-turbulent saturated state. However, turbulence is definitely in the non-linear regime and it is exhibited only in situations where a large growth of perturbations switches the system over to the non-linear regime. Since our present goal is to understand the possible origin of hydrodynamic turbulence, we consider those situations where large energy growth leads to non-linearity.

The paper is organized as follows. In the next section, we first recall the perturbation established previously (Mukhopadhyay 2006) due to secondary disturbance in the Keplerian flow and then discuss the range of corresponding Reynolds number and the associated solutions. Subsequently, we estimate the corresponding turbulent viscosity of hydrodynamic origin in Section 3. We end in Section 4 by discussing implications of our results.

2 PERTURBATION AND RANGE OF REYNOLDS NUMBER

Considering a two-dimensional velocity perturbation $\mathbf{w} = (w_x(x, y, z, t), w_y(x, y, z, t), 0)$, and pressure perturbation $p_p(x, y, z, t)$ in a small section of the Keplerian shear flow/disk, the linearized Navier-Stokes and continuity equations for an incompressible fluid with plane background shear in the presence of a Coriolis component can be written in dimensionless units as (see Mukhopadhyay et al. 2005 for a detailed description)

$$\frac{dw_x}{dt} = 2\Omega w_y - \frac{\partial p_p}{\partial x} + \frac{1}{Re} \nabla^2 w_x, \quad (1)$$

$$\frac{dw_y}{dt} = \Omega(q-2)w_x - \frac{\partial p_p}{\partial y} + \frac{1}{Re} \nabla^2 w_y, \quad (2)$$

$$\frac{\partial w_x}{\partial x} + \frac{\partial w_y}{\partial y} = 0. \quad (3)$$

We consider the standard no-slip boundary condition such that $w_x = w_y = 0$ at $x = \pm 1$ and according to the choice of variables in the coordinate system, $\Omega = 1/q$. Here (x, y, z) is a local Cartesian coordinate system centered at a point (r, ϕ) in the disk (Mukhopadhyay et al. 2005) such that $dr = x$ and $rd\phi = y$.

When the Reynolds number is very large, the solution of Equations (1), (2) and (3) are given by (Mukhopadhyay et al. 2005)

$$w_x = \zeta \frac{k_y}{l^2} \sin(k_x x + k_y y), \quad w_y = -\zeta \frac{k_x}{l^2} \sin(k_x x + k_y y), \quad (4)$$

where ζ is the amplitude of the vorticity perturbation, k_x and k_y are the components of the primary perturbation wavevector and $l = \sqrt{k_x^2 + k_y^2}$. Under this *primary perturbation*, the flow velocity and pressure are modified to

$$\mathbf{U} = \mathbf{U}^p + \mathbf{w} = (w_x, -x + w_y, 0) = \mathbf{A} \cdot \mathbf{d}, \quad \bar{P} = \bar{p} + p_p, \quad (5)$$

where \mathbf{U}^p and \bar{p} are background velocity and pressure respectively, and \mathbf{A} is a tensor of rank 2. Here $k_x = k_{x0} + k_y t$, which is basically the radial component of the primary perturbation wavevector, varies from $-\infty$ to a small number, where k_{x0} is a large negative number: $|k_{x0}| \sim Re^{1/3} \sim t_{\max}$ (Mukhopadhyay et al. 2005).

Now we concentrate on a further small patch of the primarily perturbed flow such that the spatial scale is very small compared to the wavelength of the primary perturbation satisfying $\sin(k_x x +$

$k_y y) \sim k_x x = f \lesssim 1$. In fact, $f \sim 1$ close to the boundary of the patch when $y \rightarrow 0$ and $2\pi/k_y$, and at an intermediate location $f \ll 1$. As $|k_x|$ varies from a large number to close to unity, the size of the primary perturbation box in the x -direction is $1/k_x \lesssim 1$, when $k_y \sim 1$ is fixed. Hence, this further small patch must be confined to a region: $-a \lesssim x \lesssim a$, when $f/|k_{x0}| \lesssim a \lesssim f$. Clearly, in this patch, \mathbf{U} in Equation (5) describes a flow having generalized elliptical streamlines with $\epsilon = (k_x/l)^2$, a parameter related to the measure of eccentricity², running from 0 to 1 as the perturbation evolves. It was already shown (Mukhopadhyay 2006) that a secondary perturbation in this background may grow exponentially, leading to the flow becoming unstable. We use this unstable flow in Section 3, which was extensively discussed earlier (Mukhopadhyay 2006), to derive ν_t and α .

Since we focus on the secondary perturbation at a small patch of the primarily perturbed shearing box, the variation of the primary perturbation appears insignificant in the patch compared to that of the secondary one. Depending on the primary perturbation wavevector at a particular instant, the size of the secondary patch is appropriately adjusted. In fact, ϵ varies very slowly and marginally deviates from unity in the time interval when k_x varies from k_{x0} (large negative) to, say, -10 . Even when k_x tends to -3 , ϵ only changes to ~ 0.9 . Therefore, ϵ and thus \mathbf{A} practically remain constant.

2.1 Range of Reynolds Number

Due to the consecutive choice of small boxes/patches, the Reynolds number in the secondary flow is restricted to a particular choice of that in the primary flow. Here in the interest of clarity, we work with the original dimensioned units. The Reynolds number at the primary box is defined as

$$Re_p = \frac{U_0 L}{\nu} = \frac{q\Omega_0 L^2}{\nu}, \quad (6)$$

where $2L$ is the box size in the x -direction and $2U_0$ is the relative velocity of the fluid elements in the box between two walls along the y -direction. Now we recall the secondary perturbation at a smaller patch, extending from $-L_s$ to $+L_s$, such that $|L_s| \sim aL$. To meet our requirement of $\sin(k_x x + k_y y) \sim k_x x + k_y y$, we are reminded that the small patch size needs to be adjusted. Therefore, the Reynolds number at the secondary box is given by

$$Re_s = \frac{q\Omega_0 L_s^2}{\nu} \sim \frac{q\Omega_0 a^2 L^2}{\nu}. \quad (7)$$

Hence,

$$\frac{Re_p}{Re_s} \sim \frac{1}{a^2} \sim \frac{k_x^2}{f^2}. \quad (8)$$

At the beginning of the primary perturbation, $k_x = k_{x0}$ and thus $\epsilon = 1$. At this stage, the secondary box size $L_s = Lf/k_{x0}$ and $Re_p \gtrsim k_{x0}^2 Re_s$. With time, k_x decreases in magnitude but ϵ deviates little from unity until $k_x \sim -3$ when $\epsilon = 0.9$. Hence \mathbf{A} can be considered approximately constant as described above. At this stage, $Re_p \geq 9 Re_s$, which is at least an order of magnitude higher than Re_s . If the energy growth due to the primary perturbation is maximized for $k_x = k_{x,\min} = \pi$ (Mukhopadhyay et al. 2005), then the range of Re for the secondary perturbation is given by

$$Re_p f^2 / k_{x0}^2 \lesssim Re_s \lesssim Re_p f^2 / 10.$$

At $k_x = \pi$, Re_s is at least an order of magnitude lower than Re_p . When $k_{x,\min} = 1$, $Re_p \sim Re_s$ for $f \sim 1$. In general

$$Re_p f^2 / k_{x0}^2 \lesssim Re_s \lesssim Re_p f^2 / k_{x,\min}^2.$$

² Note that ϵ is a parameter related to the measure of eccentricity but not the eccentricity itself.

2.2 Solution

Following previous work (Mukhopadhyay 2006), the general solution for the evolution of the secondary perturbation in the flow discussed above can be written in terms of Floquet modes

$$u_i(t) = \exp(\sigma t) f_i(\phi) \exp[i(k_1 x + k_2 y + k_3 z)], \quad (9)$$

where $\phi = \varpi t$, $f_i(\phi)$ is a periodic function having period $T = 2\pi/\varpi$, σ is the Floquet exponent, and k_1, k_2 , and k_3 are the components of the wavevector of the secondary perturbation. Note that σ is different at different ϵ values. Clearly, if σ is positive, then the system will be unstable. The detailed solutions were discussed elsewhere (Mukhopadhyay 2006), so we will not repeat them here.

In principle, k_x varies with time and thus so does \mathbf{A} . Thus, generalizing Equation (9) for a (slowly) varying \mathbf{A} , we obtain

$$u_i(t) = \exp\left(\int \sigma(t) dt\right) f_i(\phi) \exp[i(k_1 x + k_2 y + k_3 z)], \quad (10)$$

where $\phi = \int \varpi(t) dt$. Equations (9) and (10) practically describe the solutions for the entire parameter regime exhibiting elliptical vortices, which are very favorable to trigger the elliptical instability.

For the present purpose, the physically interesting quantity is the energy growth of the perturbation, which is given by

$$G = \frac{|u_i(t)|^2}{|u_i(0)|^2} = \exp[2\Sigma(t)] \frac{f_i^2(\phi)}{f_i^2(0)}, \quad (11)$$

where $\Sigma(t) = \int \sigma(t) dt$ and $t = (k_x - k_{x0})/k_y$. As $k_x(t)$ varies from a large negative value, k_{x0} , to 0, t increases from 0 to $t_{\max} = -k_{x0}/k_y$. Thus, the energy growth is controlled by the quantity $\Sigma(t)$, as $f_i^2(\phi)/f_i^2(0)$ simply appears to be a phase factor. Therefore, our aim should be to evaluate Σ for various possible perturbations.

Let us specifically concentrate on the Keplerian accretion flows. Figure 1(a) shows the variation of maximum velocity growth rate, σ_{\max} , as a function of eccentricity parameter, ϵ , for the various choices of amplitude of vorticity, ζ . By ‘‘maximum’’ we refer to the quantity obtained by maximizing

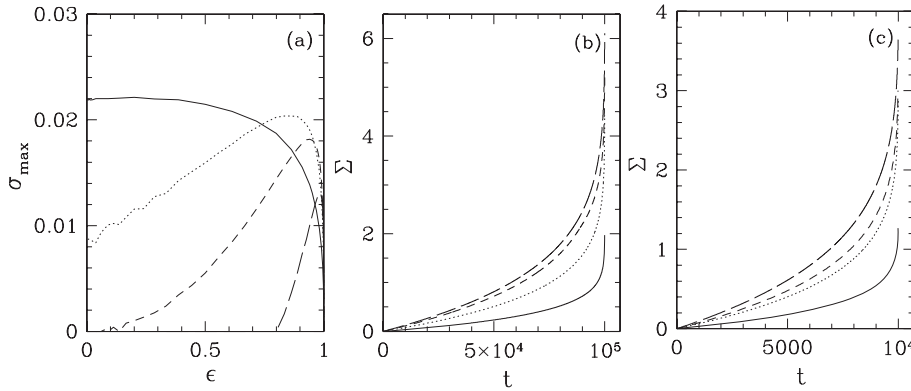


Fig. 1 (a) Variation of maximum velocity growth rate as a function of eccentricity parameter. Solid, dotted, dashed and long-dashed curves indicate the results for $\zeta = 0.01, 0.05, 0.1$, and 0.2 respectively (Mukhopadhyay 2006). (b) Variation of Σ as a function of time for $k_{x0} = -10^5$, when various curves are the same as (a). (c) Same as (b) but for $k_{x0} = -10^4$. Other parameters are $k_{y0} = 1$, $k_{10} = 0$, $|\mathbf{k}_0| = 1$, and $q = 3/2$.

over the vertical component of the wavevector, k_3 . At large ϵ (as well as large k_x), when ζ is large, the background flow structure, \mathbf{A} , is elliptical with high eccentricity. Therefore, a vertical perturbation triggers the best (maximum) growing mode into the system. However, with the decrease of ζ , \mathbf{A} approaches the structure of the plane shear and thus the growth rate decreases significantly. At this stage, the corresponding best perturbation is three-dimensional but not the vertical one.

At small ϵ (and then small k_x), when ζ is large, the eccentricity of the background elliptical flow decreases significantly, and thus the growth rate decreases. In this low eccentric flow, the best growth rate arises due to the two-dimensional perturbation. On the other hand, when ζ is small, the background reduces to that of the plane shear flow. Therefore, the growth rate increases according to the shearing effects, as described by Mukhopadhyay et al. (2005). An interesting fact to note is that, except for the case of small ϵ (k_x) with a large ζ , growth rate is maximized for the three-dimensional perturbation. Moreover, at a large ζ and a large ϵ , the best growth rate arises due to a vertical (or almost vertical) perturbation.

As the accretion time scale is an important factor, for the present purpose, the physically interesting quantity is Σ rather than σ itself. Figure 1(b) and (c) shows the variation of Σ as a function of t at various ζ values. As the perturbation evolves with time, the corresponding Σ increases. It is also clear that Σ and then corresponding growth increases with the increase of $|k_{x0}|$ (and then Re), i.e. the increase of accretion time scale, in addition to the increase of ζ . In Table 1, we enlist the approximate values of maximum growth factor, as follows from Equation (11), corresponding to $\Sigma_{\max} = \int_0^{t_{\max}} \sigma dt$, for the cases shown in Figure 1(b) and (c). When $k_{x0} = -10^4$, $Re_p \sim 10^{12}$ (as $Re_p \sim t_{\max}^3 \sim k_{x0}^3$), and from Equation (8), $Re_s(f = 1) \gtrsim 10^4$, the maximum growth factor is significant for a large amplitude of vorticity perturbation, i.e. $\zeta > 0.1$. However, the growth factor increases with the increase of Re_p and when $Re_p \sim 10^{15}$ and hence $Re_s(f = 1) \gtrsim 10^5$, it is quite significant for an amplitude of vorticity perturbations as small as 0.05. Therefore, it appears that a suitable three-dimensional secondary perturbation efficiently triggers elliptical instability and possible turbulence in rotating shear flows, including accretion disks.

Table 1 Maximum Energy Growth Corresponding to Cases Shown in Fig. 1(b) and (c)

$ k_{x0} $	ζ	Σ_{\max}	G_{\max}
10^5	0.2	6.1	2×10^5
10^5	0.1	5.2	3.3×10^4
10^5	0.05	4.43	7×10^3
10^5	0.01	1.97	52
10^4	0.2	3.65	1500
10^4	0.1	3	400
10^4	0.05	2.9	330
10^4	0.01	1.27	13

3 TURBULENT VISCOSITY

Here we attempt to quantify the turbulence by parameterizing it in terms of the viscosity. This is essential to explain any transport, as explained in Section 1, in flows like astrophysical accretion disks, where molecular viscosity is negligible.

The tangential stress at a point (r, ϕ) of a rotating flow exhibiting turbulence is

$$W_{r\phi} = \nu_t r \frac{d\Omega}{dr} = -\nu_t q \Omega, \quad (12)$$

where ν_t is the turbulent viscosity and $\Omega = \Omega_0(r/r_0)^{-q}$. Note that $q = 3/2$ for the Keplerian angular velocity profile. The perturbation described above is expected to govern the nonlinearity

after a certain time, say t_g . We also assume that the nonlinearity leads to turbulence, attributed to the fact that at the initiation of turbulence, the eddy velocity is the same as the perturbation velocity. Therefore, we obtain the averaged tangential stress due to the perturbation at $t = t_g$

$$\begin{aligned} T_{r\phi}(t_g) &\rightarrow T_{xy}(t_g) = \langle u_x u_y \rangle \\ &= \frac{k_2}{4\pi L_s} \int_{-L_s}^{+L_s} \int_0^{2\pi/k_2} u_x(t_g) u_y(t_g) dx dy, \end{aligned} \quad (13)$$

where we are reminded that the azimuthal flow is considered to be periodic in $y = 2\pi/k_2$.

Now combining Equations (12) and (13), and after some algebra we obtain

$$\bar{\nu}_t = -\frac{T_{xy}}{q\Omega\left(\frac{h}{r}\right)M}, \quad (14)$$

where $T_{xy} = \int W_{xy} dx dy$, $M = \Omega x/c_s$ and $\bar{\nu}_t$ denotes the averaged ν_t in the small section, computed here at $t = t_g$.

Without any proper knowledge of turbulence in Keplerian flows which arise in accretion disks, Shakura & Sunyaev (1973) parameterized it by a constant α considering $W_{r\phi}$ to be proportional to the sound speed, c_s , given by

$$W_{r\phi} = -\alpha c_s^2. \quad (15)$$

α is called the Shakura-Sunyaev viscosity parameter. They assumed that the small section under consideration is isotropic, so they scaled the characteristic length l_t of turbulence in terms of the largest macroscopic length scale of the disk, i.e. half-thickness h , and the eddy velocity of turbulence v_t in terms of sound speed c_s . Thus, they defined the turbulent viscosity as

$$\nu_t = \frac{l_t v_t}{3} = \alpha c_s h, \quad (16)$$

where $l_t = \alpha_l h$, $v_t = \alpha_v c_s$, and $\alpha = \alpha_l \alpha_v / 3$. Obviously $\alpha_l \leq 1$. If the turbulent velocity becomes supersonic, then a shock forms and reduces the velocity to be below the sound velocity, which assures $\alpha_v \leq 1$. Therefore, $\alpha \lesssim 1$. From Equations (14) and (16) we write

$$\bar{\alpha} = -\frac{T_{xy}}{q\Omega^2\left(\frac{h}{r}\right)^3 M r^2}, \quad (17)$$

where $\bar{\alpha}$ denotes the averaged α in the small section. Therefore, if we know the structure of the flow, then we can compute the turbulent viscosity due to various perturbations. Since we consider the size of the section to be very small, $\bar{\alpha}$ and $\bar{\nu}_t$ are effectively equivalent to α and ν_t at a particular position in the disk. Below we compute T_{xy} for the various secondary perturbations and the corresponding turbulent viscosities, at least to some approximations.

3.1 Secondary Perturbation Evolves much more Rapidly than the Primary One

From Equation (9) we can write the velocity perturbation components as

$$\begin{aligned} u_x(x, y) &= A_x e^{\sigma t} f_x(\phi) \sin(k_1 x + k_2 y + k_3 z), \\ u_y(x, y) &= A_y e^{\sigma t} f_y(\phi) \sin(k_1 x + k_2 y + k_3 z), \end{aligned} \quad (18)$$

where A_x and A_y are the amplitudes of perturbation modes, k_1 and k_2 are the radial and the azimuthal components respectively of the secondary perturbation wavevector and k_{10} and k_{20} are those at $t = 0$, A_x and A_y can be evaluated by the condition that the velocity components of the

secondary perturbation reduce to those of the primary perturbation at $t = 0$ (at the beginning of the evolution of the secondary perturbation) given by

$$\begin{aligned} A_x &= \zeta \frac{k_y}{l^2(\epsilon)} \frac{C}{f_x(0)}, & A_y &= -\zeta \frac{k_x(\epsilon)}{l^2(\epsilon)} \frac{C}{f_y(0)}, \\ C &= \frac{\sin(k_x(\epsilon)x + k_y y)}{\sin(k_{10}x + k_{20}y + k_{30}z)}, \end{aligned} \quad (19)$$

where $k_x(\epsilon) = \sqrt{\epsilon/(1-\epsilon)}k_y$, and C is of the order of unity (for details see Mukhopadhyay et al. 2005; Mukhopadhyay 2006). Therefore, from Equation (13)

$$\begin{aligned} T_{xy}(t_g) &\sim -\zeta^2 \frac{k_x(\epsilon)k_y}{2l^4(\epsilon)} e^{2\sigma t_g} D, \\ D &= C^2 \frac{f_x(\phi)f_y(\phi)}{f_x(0)f_y(0)}. \end{aligned} \quad (20)$$

Now by considering a typical case with $k_y = 0.71$, then ν_t and α can be computed as functions of ϵ (k_x), when we know the time of evolution of the secondary perturbation t_g .

Figure 2 describes ν_t and α according to Equations (14), (17) and (20) for various disk parameters. As the primary perturbation evolves, elliptical vortices form into the shearing flow which generate the turbulent viscosity under a further perturbation. Figure 2(a) shows that the viscosity varies with the eccentricity of vortices. At a very early stage when the primary perturbation is effectively a radial wave and $\epsilon \rightarrow 1$, the maximum velocity growth rate due to a secondary perturbation, σ_{\max} (shown in Fig. 1(a)), and the corresponding turbulent viscosity are very small, independent of the value of ζ . With time, the primary perturbation wavefronts are straightened out by the shear until $t = t_{\max}$, when the perturbation effectively becomes an azimuthal wave and $\epsilon \rightarrow 0$. At this stage, σ_{\max} and the turbulent viscosity due to the secondary perturbation again become zero. This feature is clearly understood from Equation (20). However, at an intermediate time when $k_x(\epsilon)$ is finite, ν_t may be ~ 0.005 even in a moderately slim disk with $h(r)/r = 0.05$, when the time of evolution of secondary perturbation $t_g = 10$. This t_g is considered to be the time at which turbulence is triggered in the system. Figure 2(b)–(d) shows the variation of ν_t and α with the eccentricity of vortices at various ζ when $t_g = 10$ –100. It is interesting to note, particularly for $t_g = 100$, that with the increase of ζ , first viscosity increases then decreases. This is understood from the underlying energy growth rate shown in Figure 1(a), when the readers are reminded that $\sigma = \sigma(\zeta, \epsilon)$. Note that the qualitative behavior of ν_t is the same as that of α . If we look at a typical case with $\zeta = 0.05$ where $\sigma = \sigma_{\max}$ at $\epsilon = 0.86$, which corresponds to $k_x = -1.76$, then α and ν_t computed at $t = t_g$ are for the cases $Re_s \lesssim Re_p \sim 10^8$.

3.2 Secondary Perturbation Over the Slowly Varying Primary Perturbation

In principle, the primary perturbation may vary with time during the evolution of the secondary perturbation. By numerical solutions, simultaneous evolution of the primary and the secondary perturbation along with the corresponding energy growth has already been discussed earlier (Mukhopadhyay 2006). For the convenience of analytical computation of viscosity, here we consider the regime of slow variation of the primary perturbation compared to the secondary one. Hence we recall Equation (10) and write the velocity perturbation components

$$\begin{aligned} u_x &\rightarrow u_{x\Sigma}(x, y) = B_x e^{\Sigma(t)} f_x(\phi) \sin(k_1 x + k_2 y + k_3 z), \\ u_y &\rightarrow u_{y\Sigma}(x, y) = B_y e^{\Sigma(t)} f_y(\phi) \sin(k_1 x + k_2 y + k_3 z), \end{aligned} \quad (21)$$

with $\phi = \int \varpi(t) dt$. The amplitudes of perturbation modes B_x and B_y can be evaluated by the initial condition of secondary perturbation. The secondary perturbation could trigger elliptical instability

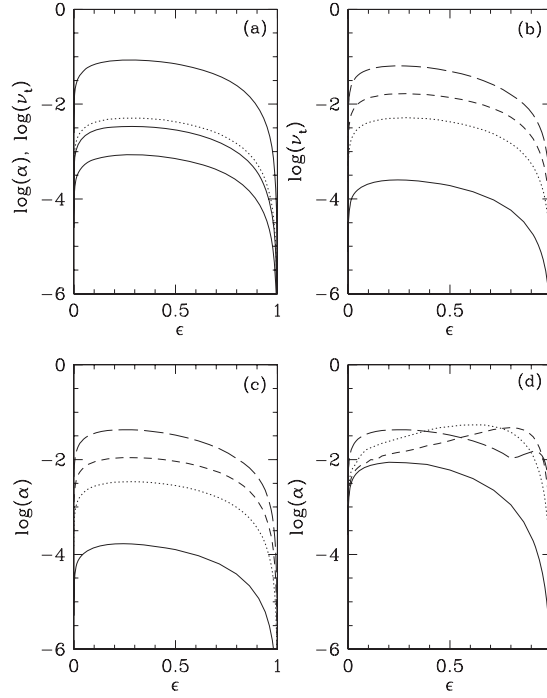


Fig. 2 Perturbation described in Sect. 3.1. (a) Variation of ν_t (dotted curve) and α (solid curve) as functions of ϵ for the $\zeta = 0.05$ case described in Fig. 1(a), when $h(r)/r = 0.01, 0.05$, and 0.1 respectively for the top, middle, and bottom curves of α ; $r = 30$, $k_y = 0.71$, and $t_g = 10$. (b) Variation of ν_t as a function of ϵ for the cases described in Fig. 1(a) with $h(r)/r = 0.05$, $t_g = 10$, and $k_y = 0.71$, when the solid, dotted, dashed, and long-dashed curves correspond to $\zeta = 0.01, 0.05, 0.1$, and 0.2 respectively with $|k_0| = 1$. (c) Same as in (b) except that α is plotted in the place of ν_t . (d) Same as in (c) except that $t_g = 100$.

only after a significant vortex forms in the flow due to the evolution of the primary one. At the beginning of the evolution of the primary perturbation $k_{x0} \rightarrow -\infty$ (we choose the cases $k_{x0} = -10^5$ and -10^4) which corresponds to $\epsilon \rightarrow 1$ and thus effectively forms a plane shear background when ζ is small (see Mukhopadhyay 2006). In the absence of a vortex, ϵ deviates from unity giving rise to a background consisting of elliptical vortices. Above a certain $\epsilon = \epsilon_c$, the secondary perturbation does not have any effect on the primarily perturbed flow and $u_{x\Sigma}$ and $u_{y\Sigma}$ reduce to the primary perturbation. We hypothesize that $\epsilon_c = 0.9999$. Hence, B_x and B_y are computed in a similar fashion as in Section 3.1 given by

$$B_x = \zeta \frac{k_y}{l^2(\epsilon_c)} \frac{C}{f_x(0)}, \quad B_y = -\zeta \frac{k_x(\epsilon_c)}{l^2(\epsilon_c)} \frac{C}{f_y(0)},$$

$$C = \frac{\sin(k_x(\epsilon_c)x + k_y y)}{\sin(k_{10}x + k_{20}y + k_{30}z)}. \quad (22)$$

Hence, from Equation (13), the stress tensor

$$T_{xy}(t_{\max}) \sim -\zeta^2 \frac{k_x(\epsilon_c)k_y}{2l^4(\epsilon_c)} e^{2\Sigma_{\max} D},$$

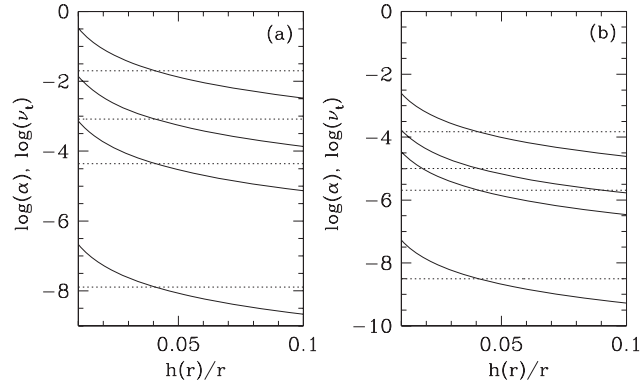


Fig. 3 Perturbation described in Sect. 3.2. Variations of ν_t (dotted curve) and α (solid curve) as functions of $h(r)/r$ for cases shown in Fig. 1(b) and (c), when the curves from top to bottom correspond to $\zeta = 0.2, 0.1, 0.05$, and 0.01 with $r = 30$ for (a) $k_{x0} = -10^5$, and (b) $k_{x0} = -10^4$. Other parameters are $k_y = 1$, and $\epsilon_c = 0.9999$.

$$D = C^2 \frac{f_x(\phi) f_y(\phi)}{f_x(0) f_y(0)} \quad (23)$$

where k_x reduces to zero at $t = t_{\max}$, which corresponds to the beginning of turbulence when $\Sigma = \Sigma_{\max}$.

It is found from Figure 3 that in a thin disk with $h(r)/r = 0.01$, α at $r = 30$ may be as high as $\gtrsim 0.1$ for $k_{x0} = -10^5$ when ζ is very large. Although the viscosity decreases with the decrease of ζ , α still may be ~ 0.001 when $\zeta = 0.05$. The turbulent viscosity decreases in a considerably thicker disk, but still $\alpha \sim 0.003$ at $h(r)/r = 0.1$ when $\zeta = 0.2$. For $\zeta \geq 0.1$, $\nu_t \gtrsim 0.001$ when $k_{x0} = -10^5$. The values of ν_t and α both decrease when $|k_{x0}|$ decreases to 10^4 , which is expected from Table 1 as well. In this case, a significant turbulent viscosity is only generated at a large $\zeta = 0.2$.

4 IMPLICATIONS AND DISCUSSION

The above results verify that in a range of ϵ , the three-dimensional growth rate due to a secondary perturbation in rotating shear flow of the Keplerian kind is always real and positive and the corresponding growth may be exponential and significant enough, at least for a suitable choice of ζ and/or Re , to trigger non-linearity and subsequent plausible turbulence in the flow time scale. With the increase of k_{x0} ($\sim Re_p^{1/3}$), the effect due to elliptical instability increases, and thus corresponding growth increase too.

Since this growth is the result of a three-dimensional perturbation, the underlying perturbation effect should survive even in the presence of viscosity. There are many important natural phenomena where the Reynolds number is very large. In astrophysical accretion disks, which have potential applications described in the present paper, Re could always be $\gtrsim 10^{10}$ because of their very low molecular viscosity. Therefore, the present mechanism is certainly applicable to such disk flows to resolve *the puzzle of their turbulence* when it is especially cold and neutral in charge and thus not a very plausible candidate for magnetorotational instability. On the other hand, we suggest that the subcritical transition to turbulence in Couette flow may be the result of secondary perturbation which triggers elliptical instability modes in the system.

We have tried to estimate the corresponding hydrodynamic turbulent viscosity. We have aimed to quantify the amount of turbulence in this model by using the perturbations as the source of turbu-

lence. We report here an observable range of viscosity obtained for the typical thin accretion disks and with reasonable values of flow vorticity. In place of $r = 30$, if we choose to place the shearing box at a large distance from the central object, say at $r = 500$, then the computed α naturally decreases three orders of magnitude [see Eq. (17)]. We show, by an extensive analysis, how the viscosity depends on the aspect ratio (h/r) of the flow. The values of ν_t and α increase quite rapidly as the disk becomes thinner. From Equations (14) and (17), and with the results given in Figures 2 and 3, we find that it still might be as large as 10^{-4} for a thin disk even at a large distance, say, $r = 500$.

While some earlier laboratory experiments (e.g. Richard & Zahn 1999) predicted a sub-critical transition to turbulence and then transport in hydrodynamical shear flows like accretion disks, experiments by Ji et al. (2006) have argued against this prediction. Non-detection of turbulence and then any angular momentum transport of a purely hydrodynamic origin could be due to the following factors. The maximum Reynolds number in this experiment is 2×10^6 whereas the cold disks, such as the protoplanetary disks, have Reynolds number $\sim 10^{12}$. However, the critical Reynolds number for these systems could be $\sim 10^6 - 10^7$ or more. It can be easily understood with a very simple example that when Re increases, the amplitude of vortices increases, which is indeed clear from figures 7 and 8 given by Mukhopadhyay et al. (2005). Let us consider a 2D perturbation in an inviscid incompressible flow where the vorticity $\nabla \times \mathbf{v}$ is exactly conserved, when $\mathbf{v} = \hat{i}v_x + \hat{j}v_y$. Therefore, at $t = t_{\max} = t_g$, when the perturbation growth is maximum at $t = t_{\max}$, the amplitude of vorticity $\zeta \sim |lv| \sim Re^{1/3}$. Since ν_t and α are directly proportional to ζ^2 , they scale as $Re^{2/3}$ at $t = t_{\max} = t_g$. Therefore, if Re decreases three orders of magnitude, then ν_t decreases by two orders. Moreover, the perturbation stabilizes at a thicker disk. Indeed, we find that the viscosity decreases as $h(r)/r$ increases. The dimension of confined liquid in the experiments by Ji et al. (2006) may not be typical of astrophysical disks or rings, when they may have a large aspect ratio ~ 2 , whereas the astrophysical disks and ring systems are normally thin (with aspect ratio ≤ 1). Obviously, a huge gap exists between experimental set ups and real observations.

By numerical simulations, the formation and evolution of vortices in a hydrodynamic shearing-sheet have already been studied by Johnson & Gammie (2005) and they suggested it to be a possible mechanism for angular momentum transport in low-ionization disks at high resolution. It has been argued that there must be a mechanism to inject vorticities into the disk, and the vortices must not decay rapidly due to three-dimensional instabilities, in order to sustain the transport. We show that the vortices may be sustained in three-dimensions, at least on the time scale of interest, where this is applicable for accretion disks. Indeed, Cuzzi and his collaborators (Cuzzi 2007; Ormel et al. 2008) have argued, by numerical simulations, that the elliptical instability may lead to turbulence to form the dusty gas surrounding a young star. Also, the vortex generation and then the angular momentum transport have been shown to occur in unmagnetized protoplanetary disks (de Val-Borro et al. 2007) by hydrodynamic turbulence. However, other simulations (Shen et al. 2006) do not find significant transport. The non-occurrence of significant transport in simulations, in our view, is due to lack of resolution needed to capture the turbulence. Indeed, the later authors have mentioned that for their calculations, it is difficult to define an effective Reynolds number, since the numerical dissipation is a steep function of resolution. With a particular non-linear solution, Balbus & Hawley (Balbus & Hawley 2006) have shown that perturbation decays asymptotically. They have also argued that as the nonlinear term in the equation for the incompressible flow itself explicitly vanishes, the solution cannot lead to nonlinearity and subsequent turbulence. However, this does not guarantee that every solution follows this model. Balbus & Hawley themselves have also mentioned that secondary instabilities may still spoil their conclusion. Indeed, the coupling between the secondary and primary modes as shown earlier does not allow the nonlinear term to vanish, resulting in a possible nonlinear transition to turbulence (Mukhopadhyay 2006).

It is interesting to note that the modal instability via the bypass mechanism (and with a subsequent secondary perturbation superimposed) arises in these systems from a subtle interplay of the non-normality of the perturbation modes and the non-linearity of the Navier-Stokes equation; this

in turn gives rise to the turbulence in the system. As the turbulence and corresponding transport are inevitable in these systems, the corresponding α may not simply be inversely proportional to the critical Reynolds number (as predicted earlier (Lesur & Longaretti 2005)). Previous theoretical studies (Mukhopadhyay et al. 2005) have shown that the Keplerian flow may render a transition to the turbulent regime at a Reynolds number $\sim 10^6$ and turbulence might have just started at this critical value. It should now be checked whether all shear flows, exhibiting subcritical turbulence in the laboratory, do exhibit large growth due to secondary perturbation.

Acknowledgements This work is partly supported by a project, Grant No. SR/S2HEP12/2007, funded by Department of Science and Technology, India.

References

- Balbus, S. A., & Hawley, J. F. 2006, *ApJ*, 652, 1020
 Bayly, B. J. 1986, *Phys. Rev. Lett.*, 57, 2160
 Bech, K. H., & Andersson, H. I. 1997, *Journal of Fluid Mechanics*, 347, 289
 Blaes, O. M., & Balbus, S. A. 1994, *ApJ*, 421, 163
 Butler, K. M., & Farrell, B. F. 1992, *Physics of Fluids*, 4, 1637
 Chagelishvili, G. D., Zahn, J., Tevzadze, A. G., & Lominadze, J. G. 2003, *A&A*, 402, 401
 Craik, A. D. D. 1989, *Journal of Fluid Mechanics*, 198, 275
 Craik, A. D. D., & Criminale, W. O. 1986, *Royal Society of London Proceedings Series A*, 406, 13
 Criminale, W. O., Jackson, T. L., & Joslin, R. D. 2003, *Theory and Computation of Hydrodynamic Stability*, eds. W. O. Criminale, T. L. Jackson, & R. D. Joslin
 Cuzzi, J. 2007, *Nature*, 448, 1003
 de Val-Borro, M., Artymowicz, P., D'Angelo, G., & Peplinski, A. 2007, *A&A*, 471, 1043
 Gammie, C. F., & Menou, K. 1998, *ApJ*, 492, L75
 Hellberg, C. S., & Orszag, S. A. 1988, *Physics of Fluids*, 31, 6
 Ji, H., Burin, M., Schartman, E., & Goodman, J. 2006, *Nature*, 444, 343
 Johnson, B. M., & Gammie, C. F. 2005, *ApJ*, 635, 149
 Kerswell, R. R. 2002, *Annual Review of Fluid Mechanics*, 34, 83
 Landman, M. J., & Saffman, P. G. 1987, *Physics of Fluids*, 30, 2339
 Le Dizès, S., Rossi, M., & Moffatt, H. K. 1996, *Physics of Fluids*, 8, 2084
 Lesur, G., & Longaretti, P. 2005, *A&A*, 444, 25
 Menou, K., & Quataert, E. 2001, *ApJ*, 552, 204
 Mukhopadhyay, B. 2006, *ApJ*, 653, 503
 Mukhopadhyay, B. 2008, *International Journal of Modern Physics D*, 17, 467
 Mukhopadhyay, B., Afshordi, N., & Narayan, R. 2005, *ApJ*, 629, 383
 Ormel, C. W., Cuzzi, J. N., & Tielens, A. G. G. M. 2008, *ApJ*, 679, 1588
 Pierrehumbert, R. T. 1986, *Physical Review Letters*, 57, 2157
 Reddy, S. C., & Henningson, D. S. 1993, *Journal of Fluid Mechanics*, 252, 209
 Richard, D., & Zahn, J. 1999, *A&A*, 347, 734
 Schmid, P. J., & Henningson, D. S. 2001, *Stability and Transition in Shear Flows* (New York: Springer-Verlag)
 Shakura, N. I., & Sunyaev, R. A. 1973, *A&A*, 24, 337
 Shen, Y., Stone, J. M., & Gardiner, T. A. 2006, *ApJ*, 653, 513
 Trefethen, L. N., Trefethen, A. E., Reddy, S. C., & Driscoll, T. A. 1993, *Science*, 261, 578
 Umurhan, O. M., & Regev, O. 2004, *A&A*, 427, 855
 Waleffe, F. 1990, *Physics of Fluids*, 2, 76